



RESEARCH ARTICLE

NEUROSCIENCE

Retrograde endocannabinoid signaling at inhibitory synapses in vivo

Barna Dudok^{1,2,*†}, Linlin Z. Fan^{3†}, Jordan S. Farrell^{2,4,5}, Shreya Malhotra², Jesslyn Homidan², Doo Kyung Kim³, Celestine Wenardy³, Charu Ramakrishnan⁶, Yulong Li⁷, Karl Deisseroth^{3,8,9}, Ivan Soltesz²

Endocannabinoid (eCB)-mediated suppression of inhibitory synapses has been hypothesized, but this has not yet been demonstrated to occur in vivo because of the difficulty in tracking eCB dynamics and synaptic plasticity during behavior. In mice navigating a linear track, we observed location-specific eCB signaling in hippocampal CA1 place cells, and this was detected both in the postsynaptic membrane and the presynaptic inhibitory axons. All-optical in vivo investigation of synaptic responses revealed that postsynaptic depolarization was followed by a suppression of inhibitory synaptic potentials. Furthermore, interneuron-specific cannabinoid receptor deletion altered place cell tuning. Therefore, rapid, postsynaptic, activity-dependent eCB signaling modulates inhibitory synapses on a timescale of seconds during behavior.

Strong depolarization of neurons can induce a transient suppression of their inhibitory synaptic inputs in acute brain slices (1, 2). Such retrograde, activity-dependent suppression of GABAergic synapses, referred to as depolarization-induced suppression of inhibition (DSI), is mediated by endocannabinoid (eCB) signaling (3–5). In vitro studies have shown that robust postsynaptic calcium (post-Ca) increase during DSI

triggers eCB synthesis and the retrograde activation of cannabinoid type-1 receptors (CB₁s), which in turn suppresses GABA release. In the CA1 region of the hippocampus, the highest CB₁ expression is found on axons of perisomatically projecting GABAergic basket cells that also express cholecystinin (CCKBCs) (6–8). Conversely, the other major basket cell type, parvalbumin-expressing basket cells (PVBCs), do not express CB₁s. Correspondingly, DSI is

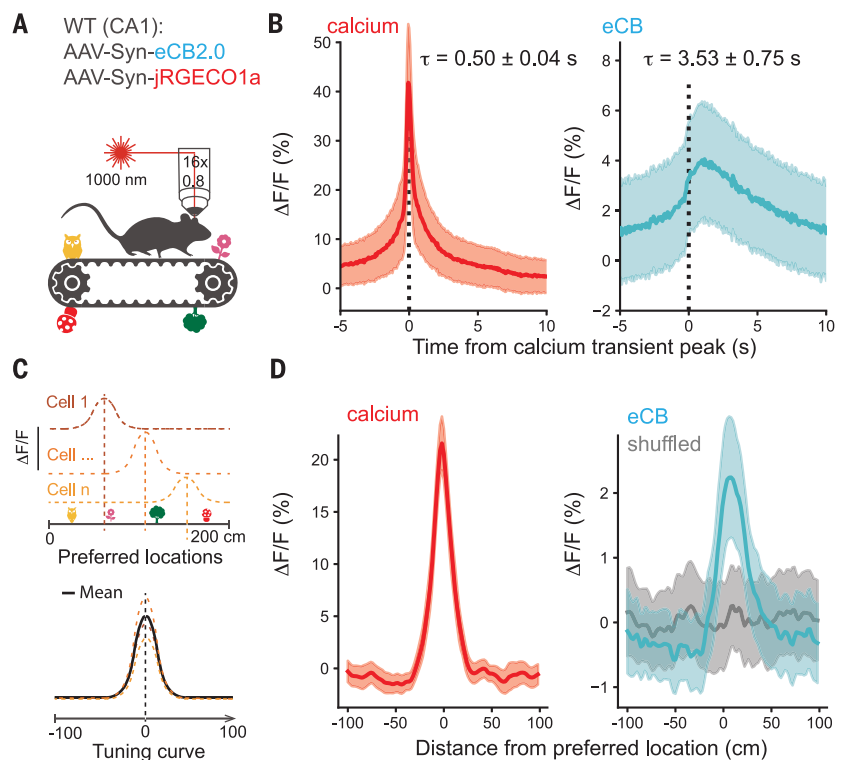
maximally potent at CCKBC inputs to pyramidal cells and is capable of completely muting these synapses (9, 10).

DSI has been hypothesized to also occur in vivo, but the specific neuronal activity patterns that give rise to DSI remain unknown (11). When mammals navigate their environment, individual hippocampal pyramidal cells discharge at specific place fields (11, 12), and several observations are consistent with the possibility that place cell firing in behaving animals may engage a DSI-like phenomenon. In vitro, externally imposed place cell-like activity can drive DSI (13), and disinhibition of the postsynaptic cells by DSI can facilitate excitatory synapse plasticity (14, 15). In vivo, place cell formation is supported by reduced inhibition (16, 17). A potential role of DSI in hippocampal place field properties has been proposed

¹Departments of Neurology and Neuroscience, Baylor College of Medicine, Houston, TX 77030, USA. ²Department of Neurosurgery, Stanford University, Stanford, CA 94305, USA. ³Department of Bioengineering, Stanford University, Stanford, CA 94305, USA. ⁴F.M. Kirby Neurobiology Center and Rosamund Stone Zander Translational Neuroscience Center, Boston Children's Hospital, Boston, MA 02115, USA. ⁵Department of Neurology, Boston Children's Hospital, Harvard Medical School, Boston, MA 02115, USA. ⁶Cracking the Neural Code (CNC) Program, Stanford University, Stanford, CA 94305, USA. ⁷State Key Laboratory of Membrane Biology, School of Life Sciences, Peking University, Beijing 100871, China. ⁸Department of Psychiatry and Behavioral Sciences, Stanford University, Stanford, CA 94305, USA. ⁹Howard Hughes Medical Institute, Stanford, CA 94305, USA. *Corresponding author. Email: barna.dudok@bcm.edu †These authors contributed equally to this work.

Fig. 1. Rapid eCB signaling in the hippocampus in vivo.

(A) GRAB_{eCB2.0} and jRGECO1a were expressed in CA1 neurons. Head-fixed mice ran on a linear treadmill during multiphoton imaging. (B) Event-aligned average single-cell calcium and eCB responses during calcium transients. Plot shows mean responses (line) ± SEM (shaded area) for $n = 4$ sessions from $n = 4$ vehicle-treated mice, 607 ± 241 ROIs per session, and 5.2 ± 1.1 peaks per ROI. Labels show decay time constants of exponential fits. (C) Analysis of place cells. Average tuning curves (solid black line) were calculated for each session by aligning location-averaged place cell traces on their preferred location. (D) Average spatial tuning curves (±SEM) are shown centered on the preferred location of place cells (red indicates calcium) together with the tuning curves of eCB signals from the same cells (blue) or after shuffling cells within sessions (gray). One-sided, one-sample t test with alternative hypothesis $\mu > 0$: $P = 5.67 \times 10^{-5}$, $n = 4$ male mice; shuffle: $P = 0.88$. Plots show average tuning curves (line) ± SEM (shaded area), $n = 4$ sessions from $n = 4$ drug-naïve mice and 161 ± 35 place cell ROIs per session.



(18); however, the steps that would underlie a retrograde, eCB-mediated, DSI-like plasticity in vivo have remained speculative, and the hypothesis that DSI contributes to place cell disinhibition has remained untested. Here, we used optical methods in mice navigating a linear track to test (i) whether place cell activity in behaving animals is sufficient to trigger eCB synthesis in the postsynaptic cell, (ii) whether eCB signals affect presynaptic CB₁s on GABAergic terminals in vivo, and (iii) whether DSI-like plasticity can modulate place cell activity patterns.

Location-specific eCB signaling by place cells

The genetically encoded G protein-coupled receptor activation based eCB reporter GRAB_{eCB2.0} enables the recording of eCB dynamics with high spatial resolution in vivo (19, 20). eCB mobilization during DSI depends on post-Ca influx (27). To characterize eCB signaling related to calcium transients, we expressed GRAB_{eCB2.0} and the red-shifted calcium sensor jRGECO1a (22) in CA1 neurons. We performed two-photon dual calcium and eCB imaging in the pyramidal layer while mice ran several laps on a linear treadmill track with tactile cues (Fig. 1A) (23). We segmented regions of interest (ROIs) corresponding to neuronal somata (most of which in the pyramidal layer are expected to belong to pyramidal cells) (24) and measured calcium

and eCB signals in the same ROIs. We analyzed calcium transients by finding peaks on traces of fluorescence change over baseline ($\Delta F/F$) (Fig. 1B). Transient eCB signals were detected concomitant with calcium peaks (Fig. 1B), with a peak delayed by 1.04 ± 0.16 s relative to calcium and an average decay time constant of 3.53 ± 0.75 s. To investigate which eCB ligand contributes to the transients, we performed the latter analysis on datasets that we previously recorded in the presence of ligand-specific inhibitors of eCB synthesis or metabolism (20). Calcium peak-coupled eCB transients were suppressed by inhibiting the synthesis of 2-arachidonoylglycerol (2-AG), the eCB species involved in CA1 DSI in vitro (25). Furthermore, eCB transient durations were extended after we treated mice with JZL 184 to inhibit monoacylglycerol lipase (MGL) and thus 2-AG degradation (25, 26) (fig. S1, A to C). Conversely, manipulations altering the synthesis or degradation of the other major eCB species, anandamide (AEA), had no effect on the in vivo eCB transients (fig. S1, D to F).

Next, to investigate eCB dynamics specifically in place cells, we identified place cells by calculating location-specific average calcium signals (Fig. 1C). Average eCB signals were elevated around the same track locations where calcium was high in the same individual place cells (Fig. 1D). These results indicate that eCB

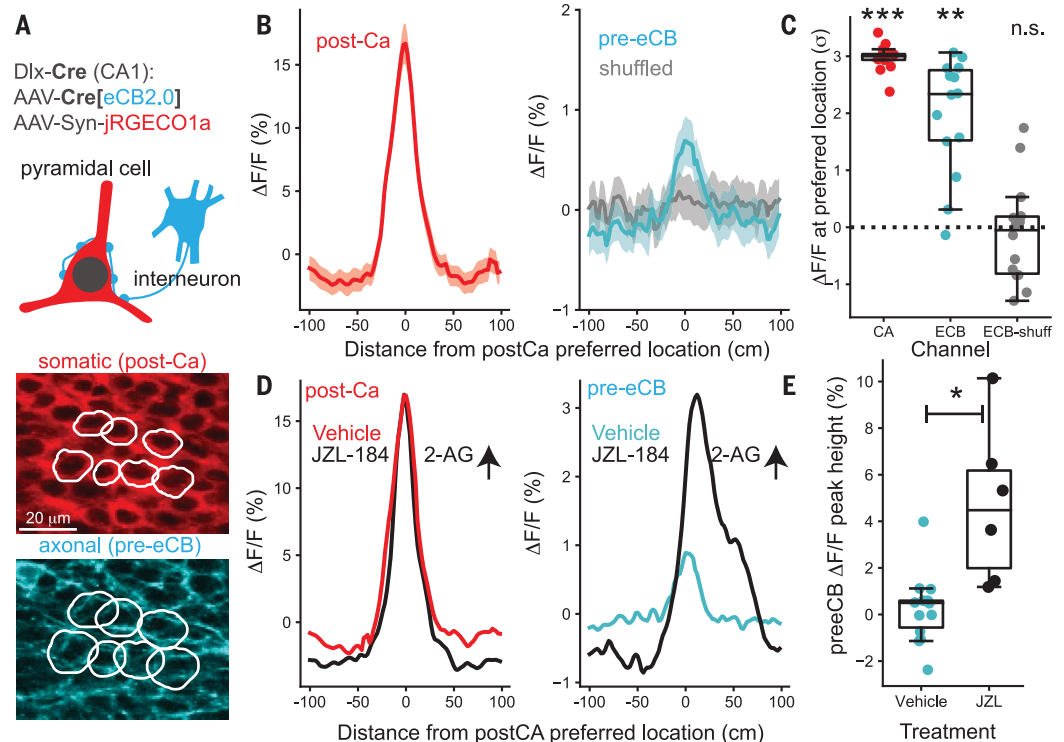
mobilization in place cells during exploration is specific to the cell's preferred location. By contrast, non-place cells had lower calcium and accompanying eCB transient amplitudes compared with place cells in the same field of view (fig. S1G).

Although the molecular mechanisms of retrograde eCB transport are not precisely understood, there is general agreement that DSI requires the postsynaptically generated eCBs to engage presynaptic CB₁s on interneuronal terminals impinging on the activated neuron (4, 27). Thus, we specifically allowed the expression of GRAB_{eCB2.0} only in interneurons using *Dlx5/6-Cre* transgenic mice (28) to enable presynaptic eCB measurements (fig. S2A). The distribution of GRAB_{eCB2.0}, a chimera of CB₁ and a green fluorescent protein variant, resembled membrane-enriched CB₁ targeting (29) in interneuron axon terminals, with no detectable postsynaptic expression in principal cells and relatively low expression in interneuron somata (fig. S2, B to F).

For simultaneously imaging somatic calcium and axonal eCB transients, we combined interneuronal GRAB_{eCB2.0} and pan-neuronal, red-shifted calcium sensor expression (Fig. 2A and fig. S2E). We generated somatic, putatively post-Ca ROI sets as above and measured nearby axonal, putatively presynaptic eCB (pre-eCB) signals after enlarging the somatic

Fig. 2. Spatially tuned presynaptic eCB signals in the hippocampus in vivo.

(A) Labeling strategy for in vivo imaging. Interneuronal GRAB_{eCB2.0} and pan-neuronal jRGECO1a expression were combined. Bottom panels show the segmentation approach. Neuron cell bodies were segmented in the jRGECO1a channel (post-Ca). The ROIs were enlarged by binary dilation for measuring signals in the neighboring axons in the GRAB_{eCB2.0} channel (pre-eCB). (B) Average spatial tuning curves (\pm SEM) are shown centered on the preferred location of place cells (red indicates calcium) together with the tuning curves of eCB signals from the corresponding pre-eCB ROIs (blue) or after shuffling ROIs within sessions (gray), $n = 18$ sessions from $n = 5$ mice and 193 ± 130 ROIs per session. (C) Quantification of signal intensity at the preferred location. Boxes indicate median \pm interquartile range; whiskers: nonoutlier range; markers: recording sessions. pre-eCB: $P = 0.002$, $n = 5$ mice ($n = 3$ males and $n = 2$ females); shuffle: $P = 0.69$. (D) Spatial tuning curves are shown after injecting mice with JZL-184 to inhibit the enzymatic breakdown of the eCB 2-AG by MGL or after vehicle injection. (E) Quantification of location-specific pre-eCB signals, $P = 0.0004$, Mann-Whitney test, $n = 14$ vehicle sessions from $n = 5$ mice and $n = 6$ JZL sessions from $n = 3$ mice.



ROIs (Fig. 2A). Similar to eCB signals measured in place cell somata (Fig. 1D), pre-eCB signals in interneuronal axons surrounding place cells were elevated at the same track locations where post-Ca was high (Fig. 2, B and C). These results indicate that place cell

activations during behavior are accompanied by eCB signaling at perisomatic inhibitory axons.

Similarly to DSI *in vitro* (30) and calcium transient-related post-eCB signals *in vivo* (fig. S1B), location-specific pre-eCB signals around

place cells were magnified by pharmacological inhibition of 2-AG degradation (Fig. 2, D and E), consistent with a prominent role of 2-AG in inhibitory axon eCB signaling while not ruling out the partial involvement of other eCBs such as AEA.

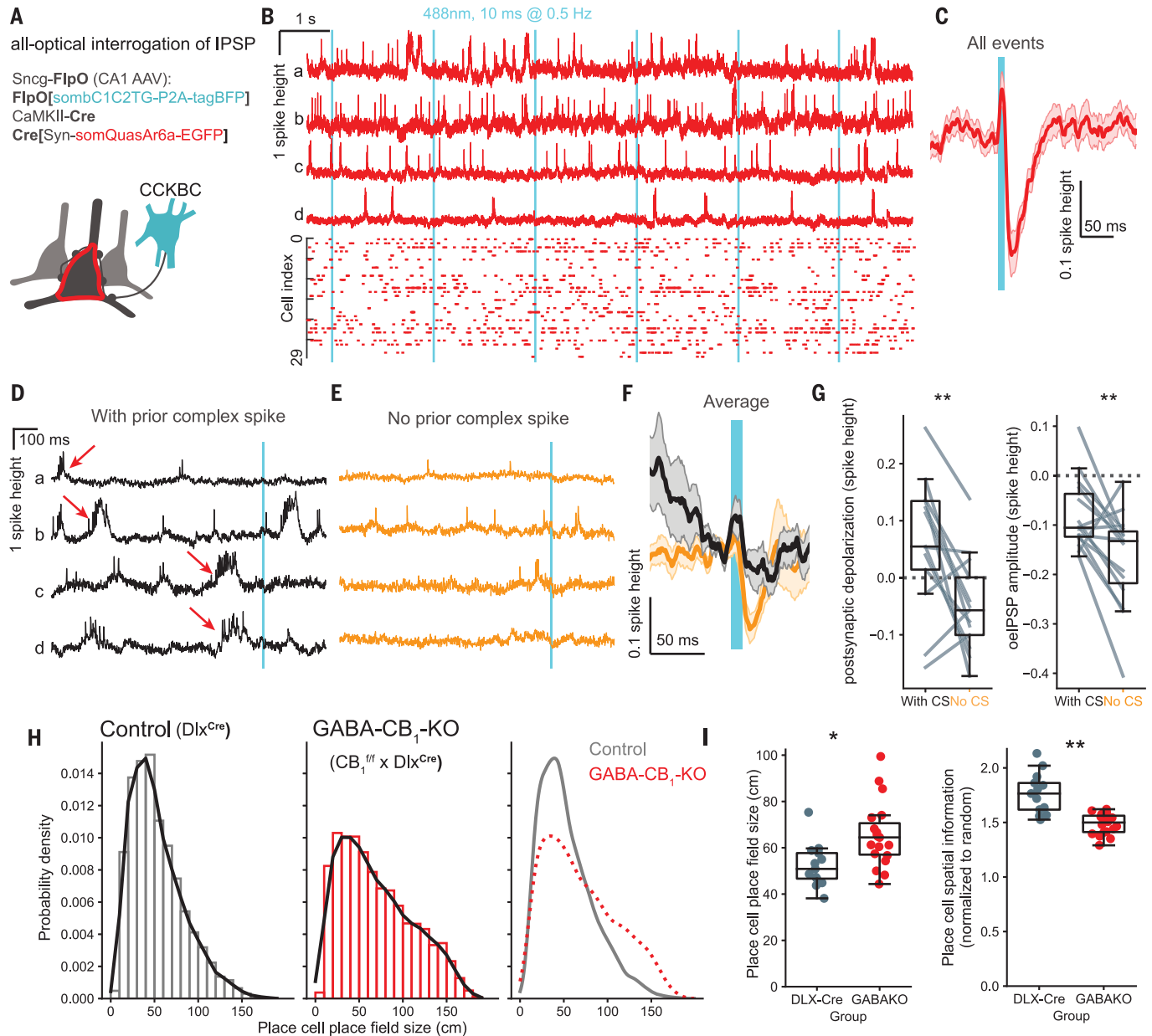


Fig. 3. Inhibitory synaptic plasticity in behaving mice. (A) Labeling strategy for the all-optical assay of CCKBC synaptic function *in vivo*. (B) Top: example unfiltered fluorescence traces from four CA1 neurons [(a) to (d)]. Bottom: spike raster ($n = 30$ neurons from $n = 5$ mice). Cyan bars indicate CCKBC photostimulation onset (488 nm, 10 ms duration, 9.5 to 20 mW/mm², 0.5 Hz). (C) Mean subthreshold postsynaptic waveforms after presynaptic CCKBC photostimulation ($n = 30$ neurons from $n = 5$ mice). (D) Unfiltered example traces of plateau-driven complex spikes (CS, red arrows) preceding photostimulation events. (E) Additional example traces from the same cells as in (D) without complex spikes occurring within 1 s before the stimulation. (F) Stimulus-triggered average (mean \pm SEM) oelPSP (black: with CS; orange: without CS). (G) Quantification of neuronal depolarization before stimulation

and oelPSP amplitudes (negative values) during trials with or without preceding complex spikes (depolarization: $P = 0.0076$, paired t test, $n = 15$ cells from $n = 4$ mice; oelPSP amplitude: $P = 0.0045$). (H) Histograms of place field sizes of individual place cells in control mice and after cell-type-specific CB₁ KO in GABAergic neurons (GABA-CB₁-KO). $n = 420 \pm 254$ place cells from $n = 5$ control and $n = 3$ GABA-CB₁-KO mice. (I) Quantification of place cell place field size and spatial information. $n = 13$ sessions from $n = 2$ male and $n = 2$ female control mice; $n = 19$ sessions from $n = 3$ male GABA-CB₁-KO mice. Markers and box plots show individual sessions (boxes: median \pm interquartile range, whiskers: nonoutlier range). Place field size: $P = 0.032$, $\chi^2(1) = 4.59$; spatial information: $P = 0.004$, $\chi^2(1) = 8.5$, linear mixed effects models and likelihood ratio test.

Postsynaptic activity-dependent modulation of inhibitory postsynaptic potentials

Retrograde eCB signaling through CB₁ inhibits CCKBC to pyramidal cell synapses in vitro (9, 31). On the basis of our results showing eCB transients time-locked to calcium transients, we expected to observe an activity-dependent modulation of CCKBC synapses. We used a CCKBC-specific (Sneg-FlpO) mouse line to test this hypothesis (32) and developed an all-optical method to study synaptic transmission between CCKBCs and postsynaptic neurons. These animals express the FlpO recombinase enzyme specifically in gamma-synuclein (Sneg)-expressing cells. Sneg is expressed selectively in CCKBCs; therefore, FlpO will be expressed specifically in this cell population in Sneg-FlpO mice. We expressed FlpO-dependent excitatory opsin (sombC1C2TG) (33) in CCKBCs and a soma-localized genetically encoded voltage indicator (GEVI, somQuasAr6a) (34) in sparsely labeled CA1 neurons in Sneg-FlpO mice (Fig. 3A and fig. S3A). We imaged GEVI in awake mice head-fixed on a spherical treadmill while activating CCKBCs with photostimulation (Fig. 3B). Brief CCKBC activation elicited time-locked CA1 neuronal hyperpolarization, consistent with optogenetically evoked inhibitory postsynaptic potentials (oeIPSP; Fig. 3C).

Plateau-driven complex spikes in CA1 pyramidal cells are particularly important for synaptic plasticity (12, 33, 35). We identified plateau-driven complex spikes with voltage imaging and then grouped the photostimulation-induced responses based on the presence or absence of complex spikes during the 1 s before the stimulus (Fig. 3, D and E). Whereas oeIPSPs were detectable in the absence of a preceding complex spike (Fig. 3E), the same postsynaptic cells showed reduced oeIPSPs after complex spikes (Fig. 3, D, F, and G). As expected, the average postsynaptic depolarization before the CCKBC stimulus was higher in the presence of complex spikes (Fig. 3G). Together, these results demonstrate a transient suppression of CCKBC inhibition after complex spikes, consistent with a DSI-like mechanism.

Interneuron cannabinoid receptors modulate place cell activity patterns

The above results provide evidence for postsynaptic neuronal activity-dependent modulation of CCKBC synapses in vivo. A suppression of inhibition could disinhibit place cells during place field traversal, contributing to location-specific place cell activity (16, 36). To determine whether preventing inhibitory synaptic eCB signaling may lead to altered place fields, we knocked out CB₁ selectively in forebrain GABAergic neurons (GABA-CB₁-KO, lacking CB₁ from perisomatic and dendritic interneurons) (28) (fig. S3B) and recorded place cell calcium signals during a spatial navigation task

as mice foraged for a water reward. Both control (Dlx-Cre) and GABA-CB₁-KO mice exhibited spatially tuned calcium signals, suggesting that CB₁ expression by GABAergic neurons is not required for place field formation per se (fig. S3, C and D). However, we observed a widening of place fields in GABA-CB₁-KO mice relative to mice with intact CB₁ expression (Fig. 3, H and I). Analyzing the properties of individual place cells revealed that in the absence of interneuron CB₁ expression, place cells were active over a larger fraction of the belt and altogether encoded less spatial information (Fig. 3I and fig. S3, C to J). In GABA-CB₁-KO mice, place cells fired less reliably lap-to-lap, and had fewer calcium transients near the preferred location (fig. S3, H and I). As a population, place cells in the GABA-CB₁-KO encoded mouse location less accurately compared with control despite the similar ratio of place cells (fig. S3, E and J). The observed changes in place cell activity patterns are consistent with the reported impaired spatial learning performance of GABA-CB₁-KO mice (37) and mice with perturbed CCKBC development (38).

In this study, we report (i) rapid eCB signals time-locked to calcium transients in hippocampal neurons including place cells, both in the postsynaptic membrane and the presynaptic inhibitory axons; (ii) modulation of CCKBC synapses correlated to past postsynaptic activity; and (iii) diminished place cell place field properties in the absence of eCB signaling at inhibitory synapses. Our results demonstrate that an eCB-mediated, DSI-like plasticity is capable of rapid modulation of inhibition in vivo on the behaviorally relevant timescale of seconds. Because of the selective expression of CB₁ at synapses of CCK-expressing but not PV-expressing interneurons, DSI may enable recently activated place cells to maintain elevated excitability without suppressing the ability of PVBC synapses to synchronize the PC population activity dynamics to theta and gamma oscillations (39, 40). Such a selective, lasting suppression of inhibition involving CB₁ signaling may also contribute to maintaining an eligibility trace for non-Hebbian activity-dependent plasticity (41).

REFERENCES AND NOTES

1. I. Llano, N. Leresche, A. Marty, *Neuron* **6**, 565–574 (1991).
2. T. A. Pitler, B. E. Alger, *J. Neurosci.* **12**, 4122–4132 (1992).
3. A. C. Kreitzer, W. G. Regehr, *J. Neurosci.* **21**, RC174 (2001).
4. R. I. Wilson, R. A. Nicoll, *Nature* **410**, 588–592 (2001).
5. T. Maejima, K. Hashimoto, T. Yoshida, A. Aiba, M. Kano, *Neuron* **31**, 463–475 (2001).
6. I. Katona et al., *J. Neurosci.* **19**, 4544–4558 (1999).
7. K. Tsou, S. Brown, M. C. Sañudo-Peña, K. Mackie, J. M. Walker, *Neuroscience* **83**, 393–411 (1998).
8. G. Marsicano, B. Lutz, *Eur. J. Neurosci.* **11**, 4213–4225 (1999).
9. C. Földy, A. Neu, M. V. Jones, I. Soltesz, *J. Neurosci.* **26**, 1465–1469 (2006).
10. S.-H. Lee et al., *J. Neurosci.* **35**, 10039–10057 (2015).
11. J. O'Keefe, J. Dostrovsky, *Brain Res.* **34**, 171–175 (1971).
12. K. C. Bittner et al., *Nat. Neurosci.* **18**, 1133–1142 (2015).
13. F. Dübucq, D. Dupret, O. Caillard, *J. Neurophysiol.* **110**, 1930–1944 (2013).

14. G. Carlson, Y. Wang, B. E. Alger, *Nat. Neurosci.* **5**, 723–724 (2002).
15. V. Chevaleyre, P. E. Castillo, *Neuron* **43**, 871–881 (2004).
16. M. Valero, A. Navas-Olive, L. M. de la Prida, G. Buzsáki, *Cell Rep.* **40**, 111232 (2022).
17. S. V. Rolotti et al., *Neuron* **110**, 783–794.e6 (2022).
18. T. F. Freund, I. Katona, D. Piomelli, *Physiol. Rev.* **83**, 1017–1066 (2003).
19. A. Dong et al., *Nat. Biotechnol.* **40**, 787–798 (2022).
20. J. S. Farrell et al., *Neuron* **109**, 2398–2403.e4 (2021).
21. Y. Hashimoto, T. Ohno-Shosaku, M. Kano, *Curr. Opin. Neurobiol.* **17**, 360–365 (2007).
22. H. Dana et al., *eLife* **5**, e12727 (2016).
23. N. B. Danielson et al., *Neuron* **91**, 652–665 (2016).
24. P. Kaifosh, J. D. Zaremba, N. B. Danielson, A. Losonczy, *Front. Neuroinform.* **8**, 80 (2014).
25. Y. Hashimoto, T. Ohno-Shosaku, T. Maejima, K. Fukami, M. Kano, *Neuropharmacology* **54**, 58–67 (2008).
26. J. Z. Long, D. K. Nomura, B. F. Cravatt, *Chem. Biol.* **16**, 744–753 (2009).
27. E. Albarran et al., *Nat. Neurosci.* **26**, 997–1007 (2023).
28. K. Monory et al., *Neuron* **51**, 455–466 (2006).
29. B. Dudok et al., *Nat. Neurosci.* **18**, 75–86 (2015).
30. B. Pan et al., *J. Pharmacol. Exp. Ther.* **331**, 591–597 (2009).
31. L. L. Glickfeld, M. Scanziani, *Nat. Neurosci.* **9**, 807–815 (2006).
32. B. Dudok et al., *Neuron* **109**, 997–1012.e9 (2021).
33. L. Z. Fan et al., *Cell* **186**, 543–559.e19 (2023).
34. H. Tian et al., *Nat. Methods* **20**, 1082–1094 (2023).
35. J. Epsztein, M. Brecht, A. K. Lee, *Neuron* **70**, 109–120 (2011).
36. S. Royer et al., *Nat. Neurosci.* **15**, 769–775 (2012).
37. Ö. Albayram, S. Passlick, A. Bilkei-Gorzo, A. Zimmer, C. Steinhäuser, *Pflügers Arch.* **468**, 727–737 (2016).
38. I. Del Pino et al., *Nat. Neurosci.* **20**, 784–792 (2017).
39. C. Varga, P. Golshani, I. Soltesz, *Proc. Natl. Acad. Sci. U.S.A.* **109**, E2726–E2734 (2012).
40. M. Bartos et al., *Proc. Natl. Acad. Sci. U.S.A.* **99**, 13222–13227 (2002).
41. A. D. Milstein et al., *eLife* **10**, e73046 (2021).

ACKNOWLEDGMENTS

We thank A. Ortiz, C. Porter, S. Linder, and K. Patron for technical and administrative support. **Funding:** This work was supported by the National Institute of Neurological Disorders and Stroke (NINDS) of the National Institutes of Health (NIH). The content is solely the responsibility of the authors and does not necessarily represent the official views of the NIH. This work was supported by the NIH (grants R01NS099457, R01NS11728, and R01NS133381 to I.S.; grant R00NS117795 to B.D.; grant K99MH132871 to L.Z.F.; and grant K99NS126725 to J.S.F.); the Knight Initiative for Brain Resilience (grant KCG-116 to I.S.); a McNair scholarship from the McNair Medical Institute at The Robert and Janice McNair Foundation to B.D.; a Helen Hay Whitney fellowship to L.Z.F.; a Burroughs Wellcome Fund Career Award at the Scientific Interface to L.Z.F.; a Stanford University Bio-X Undergraduate Summer Research Program grant to C.W.; and the National Institute of Mental Health, National Institute on Drug Abuse, National Science Foundation, Gatsby Foundation, Frensenius Foundation, AE Foundation, Tarlton Foundation, and NOMIS Foundation to K.D. **Author contributions:** Conceptualization: B.D., L.Z.F., K.D., I.S.; Formal analysis: B.D., L.Z.F.; Funding acquisition: B.D., K.D., I.S.; Investigation: B.D., L.Z.F., J.S.F., S.M., J.H., D.K., C.W., C.R.; Methodology: B.D., L.Z.F., J.S.F.; Resources: Y.L.; Supervision: K.D., I.S.; Visualization: B.D., L.Z.F.; Writing – original draft: B.D., L.Z.F., I.S.; Writing – review & editing: all authors. **Competing interests:** I.S. declares unrelated consultant activity for Actio Biosciences, CODA Biotherapeutics, MapLight Therapeutics, Praxis Precision Medicines, and Ray Therapeutics. K.D. declares unrelated consultant activity for MapLight Therapeutics and Stellaromics. The remaining authors declare no competing interests. **Data and materials availability:** All data, code, and materials are available from the authors upon reasonable request. **License information:** Copyright © 2024 the authors, some rights reserved; exclusive licensee American Association for the Advancement of Science. No claim to original US government works. <https://www.science.org/about/science-licenses-journal-article-reuse>

SUPPLEMENTARY MATERIALS

science.org/doi/10.1126/science.adk3863
Materials and Methods
Figs. S1 to S3
References (42–45)
MDAR Reproducibility Checklist

Submitted 18 August 2023; accepted 24 January 2024
10.1126/science.adk3863